

PSR J2030+3641: RADIO DISCOVERY AND GAMMA-RAY STUDY OF A MIDDLE-AGED PULSAR IN THE NOW IDENTIFIED FERMI-LAT SOURCE 1FGL J2030.0+3641

F. CAMILO^{1,2}, M. KERR^{3,4,5}, P. S. RAY^{6,7}, S. M. RANSOM⁸, S. JOHNSTON⁹, R. W. ROMANI³, D. PARENT¹⁰, M. E. DECESAR^{11,12}, A. K. HARDING¹¹, D. DONATO^{12,13}, P. M. SAZ PARKINSON¹⁴, E. C. FERRARA¹¹, P. C. C. FREIRE¹⁵, L. GUILLEMOT¹⁵, M. KEITH⁹, M. KRAMER^{15,16}, AND K. S. WOOD⁶

Accepted for publication, 2011 Nov 17

ABSTRACT

In a radio search with the Green Bank Telescope of three unidentified low Galactic latitude *Fermi*-LAT sources, we have discovered the middle-aged pulsar J2030+3641, associated with 1FGL J2030.0+3641 (2FGL J2030.0+3640). Following the detection of gamma-ray pulsations using a radio ephemeris, we have obtained a phase-coherent timing solution based on gamma-ray and radio pulse arrival times that spans the entire *Fermi* mission. With a rotation period of 0.2 s, spin-down luminosity of 3×10^{34} erg s⁻¹, and characteristic age of 0.5 Myr, PSR J2030+3641 is a middle-aged neutron star with spin parameters similar to those of the exceedingly gamma-ray-bright and radio-undetected Geminga. Its gamma-ray flux is 1% that of Geminga, primarily because of its much larger distance, as suggested by the large integrated column density of free electrons, DM = 246 pc cm⁻³. We fit the gamma-ray light curve, along with limited radio polarimetric constraints, to four geometrical models of magnetospheric emission, and while none of the fits have high significance some are encouraging and suggest that further refinements of these models may be worthwhile. We argue that not many more non-millisecond radio pulsars may be detected along the Galactic plane that are responsible for LAT sources, but that modified methods to search for gamma-ray pulsations should be productive — PSR J2030+3641 would have been found blindly in gamma rays if only $\gtrsim 0.8$ GeV photons had been considered, owing to its relatively flat spectrum and location in a region of high soft background.

Subject headings: gamma rays: observations — pulsars: individual (PSR J2030+3641)

1. INTRODUCTION

Three years after the launch of the *Fermi Gamma-ray Space Telescope*, pulsations have been detected with its Large Area Telescope (LAT) from at least 100 rotation-powered neutron stars (e.g., Abdo et al. 2010d), increasing by more than an order of magnitude the number of pulsars known to emit

above 0.1 GeV¹⁷. Nearly 20 of these are millisecond pulsars (MSPs) known independent from *Fermi*, for which rotational ephemerides obtained from radio observations were used to fold the sparse gamma-ray photons (e.g., Abdo et al. 2009a, 2010a). Another 34 have been discovered in direct pulsation searches of the gamma-ray data (e.g., Abdo et al. 2009b; Pletsch et al. 2011; Saz Parkinson et al. 2010).

Among the known non-MSP gamma-ray pulsar sample, about 75% have large values of spin-down luminosity ($\dot{E} > 10^{35}$ erg s⁻¹); the remaining 17 have lower \dot{E} and are older, with characteristic age $\tau_c = P/(2\dot{P}) \sim 0.1$ –1 Myr. Five of these are also radio emitters (two are exceedingly faint and were detected only after the gamma-ray discoveries; Camilo et al. 2009b; Pletsch et al. 2011). Almost all of these middle-aged pulsars are also known or expected to be nearby, at $d \lesssim 1$ kpc, although obviously many more similar pulsars exist at larger distances. In principle several of them could be detected in gamma rays despite a relatively low \dot{E} , because the efficiency for conversion of rotational kinetic energy into gamma rays, $\eta \equiv L_\gamma/\dot{E}$, apparently increases with decreasing \dot{E} and may approach 100% for $\dot{E} \approx 10^{33-34}$ erg s⁻¹ (see Abdo et al. 2010d; Arons 1996; Muslimov & Harding 2003).

In order to improve our understanding of pulsar emission mechanisms and evolution, it is important to identify more gamma-ray-emitting neutron stars, particularly in under-represented groups such as middle-aged pulsars. The *Fermi* LAT First Source Catalog (1FGL), based on 11 months of survey data and containing more than 600 unidentified sources (Abdo et al. 2010b), provides a path toward such discoveries (as does now 2FGL; Abdo et al. 2011a). Many

¹ Columbia Astrophysics Laboratory, Columbia University, New York, NY 10027, USA

² email: fernando@astro.columbia.edu

³ W. W. Hansen Experimental Physics Laboratory, Kavli Institute for Particle Astrophysics and Cosmology, Department of Physics and SLAC National Accelerator Laboratory, Stanford University, Stanford, CA 94305, USA

⁴ email: kerrm@stanford.edu

⁵ Einstein Fellow

⁶ Space Science Division, Naval Research Laboratory, Washington, DC 20375-5352, USA

⁷ email: Paul.Ray@nrl.navy.mil

⁸ National Radio Astronomy Observatory (NRAO), Charlottesville, VA 22903, USA

⁹ CSIRO Astronomy and Space Science, Australia Telescope National Facility, Epping NSW 1710, Australia

¹⁰ Center for Earth Observing and Space Research, College of Science, George Mason University, Fairfax, VA 22030, resident at Naval Research Laboratory, Washington, DC 20375, USA

¹¹ NASA Goddard Space Flight Center, Greenbelt, MD 20771, USA

¹² Department of Physics and Department of Astronomy, University of Maryland, College Park, MD 20742, USA

¹³ Center for Research and Exploration in Space Science and Technology (CRESTT) and NASA Goddard Space Flight Center, Greenbelt, MD 20771, USA

¹⁴ Santa Cruz Institute for Particle Physics, Department of Physics and Department of Astronomy and Astrophysics, University of California at Santa Cruz, Santa Cruz, CA 95064, USA

¹⁵ Max-Planck-Institut für Radioastronomie, Auf dem Hügel 69, 53121 Bonn, Germany

¹⁶ Jodrell Bank Centre for Astrophysics, School of Physics and Astronomy, The University of Manchester, M13 9PL, UK

¹⁷ See <https://confluence.slac.stanford.edu/display/GLAMCOG/Public+List+of+LAT+Detected+Gamma-Ray+Pulsars> for an up-to-date list.

unidentified LAT sources are being surveyed within the context of a “pulsar search consortium” that aims to efficiently organize this collaborative radio and gamma-ray work (see, e.g., Ray & Parkinson 2011). Spectacularly, many radio MSPs have recently been discovered in such searches at high Galactic latitudes ($|b| > 5^\circ$; e.g., Cognard et al. 2011; Keith et al. 2011; Ransom et al. 2011). Here we report on the first pulsar to be discovered at low Galactic latitude that is responsible for a formerly unidentified 1FGL source. PSR J2030+3641 in 1FGL J2030.0+3641 (also 2FGL J2030.0+3640), discovered with the NRAO Green Bank Telescope (GBT), is also the first non-MSP gamma-ray pulsar identified in radio searches of 1FGL sources.

2. OBSERVATIONS AND RESULTS

2.1. Radio Searches

Consistent with the properties of known gamma-ray pulsars, our first 1FGL search targets are non-variable and have spectra consistent with exponentially-cutoff power laws. In this initial small radio survey at the GBT we aimed to search along the Galactic plane, indicating a relatively high search frequency ($\gtrsim 1$ GHz) in order to minimize deleterious propagation effects in the interstellar medium and the background temperature due to Galactic synchrotron emission. At the 2 GHz frequency used, the GBT beam is $3'$ HWHM, and the 1FGL sources to be searched should therefore, ideally, have r_{95} (95% confidence level error radii) below that, after accounting for the combined statistical and estimated systematic positional uncertainties. These are strict criteria, and we searched a total of only three sources. For each we provide $(\alpha, \delta, \Delta_\theta, r_{95})$, which are respectively the R.A. and decl. of the *observed* position, its offset from the 1FGL position (we observed in late 2009, based on an interim version of the catalog), and r_{95} for the gamma-ray source: 1FGL J0224.0+6201c ($36^\circ 00', 62^\circ 04', 1', 4'$), where the “c” indicates that the measured properties of this source (including position) may not be reliable; 1FGL J1746.7–3233 ($266^\circ 70', -32^\circ 61', 3', 3'$); and 1FGL J2030.0+3641 ($307^\circ 52', 36^\circ 68', 1', 3'$).

We observed each source for 1 hr using the GUPPI spectrometer¹⁸ at a central frequency of 2 GHz. Each of 512 polarization-summed frequency channels, spanning a bandwidth of 800 MHz, were sampled every 0.164 ms before writing to disk. The flux density limit of these searches, converted to a standard search frequency of 1.4 GHz, was approximately 0.03 mJy, for an assumed pulsar duty cycle of 10% and spin period larger than a few tens of milliseconds. We analyzed the data with standard pulsar search techniques implemented in PRESTO (Ransom 2001), selecting trial dispersion measures so as to maintain ideal sensitivity up to twice the maximum Galactic DM predicted in each direction by the Cordes & Lazio (2002) electron distribution model. The data sets retained significant sensitivity to (possibly binary) MSPs up to $DM \approx 100 \text{ pc cm}^{-3}$. We therefore did the analysis in two passes, including one where we allowed for a modest amount of unknown constant acceleration (parameterized in PRESTO by $z_{\text{max}} = 50$). In the 1FGL J2030.0+3641 data, collected on 2009 November 27, we discovered on Christmas day an obvious pulsar with period $P = 0.200$ s and $DM = 247 \text{ pc cm}^{-3}$.

2.2. Radio Timing and Polarimetry of PSR J2030+3641

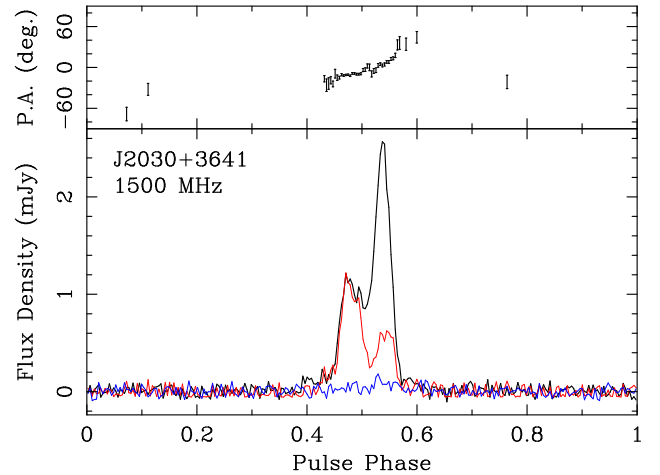


FIG. 1.— Polarimetric observation of PSR J2030+3641 at 1.5 GHz with the GBT. In the lower panel the total-intensity profile is represented by the black trace, red corresponds to linear polarization, and blue to circular. The profiles, based on a 4.5 hr integration, are displayed with a resolution of 256 bins and arbitrary phase. In the upper panel the position angle of linear polarization is displayed for bins in which the linear signal-to-noise ratio exceeds 2.2, and the PAs have been rotated to the pulsar frame using the measured $RM = +514 \text{ rad m}^{-2}$. The full pulse phase corresponds to $P = 0.200$ s.

We began regular timing observations of the new pulsar at GBT on 2010 January 8. Observing parameters were identical to those used in the search observation, although with much shorter integration times, typically 5 minutes. In this manner we measured pulse times of arrival (TOAs) on 28 separate days through 2011 April 11. Using these with TEMPO¹⁹ we obtain a phase-connected rotational ephemeris with 0.3 ms rms residual. After 5 months of radio timing, the solution was sufficient to yield an initial detection of gamma-ray pulsations (see Section 2.3). The DM measurement was improved with the aid of one additional observation centered at 1.5 GHz, and implies an uncertainty in the alignment of radio and gamma-ray pulses of only 0.7 ms.

In order to determine the polarization characteristics of PSR J2030+3641, we have used GUPPI to make three flux-calibrated full-Stokes observations of the pulsar, one each at central frequencies of 0.82 GHz (lasting for 2.3 hr), 1.5 GHz (4.5 hr), and 2 GHz (1.0 hr). We analyzed the data with PSRCHIVE (Hotan et al. 2004), and show the resulting 1.5 GHz profiles in Figure 1. The profiles at the other two frequencies are comparable, with a possible slight hint of interstellar scattering visible at 0.8 GHz. The Faraday rotation measure is $RM = +514 \text{ rad m}^{-2}$, which implies an average electron-weighted Galactic magnetic field strength along the line of sight of $2.6 \mu\text{G}$. The radio spectral index, based on the three flux density measurements, is $\alpha = -1.7 \pm 0.1$ (where $S_\nu \propto \nu^\alpha$; see Table 1).

2.3. Gamma-ray Study of PSR J2030+3641

We used “Pass 6 diffuse”-class *Fermi* LAT events (having the highest probability of being gamma-ray photons), excluding those with zenith angles $> 100^\circ$ to minimize gamma-ray emission from the Earth’s limb. The events were analyzed using the LAT *Science Tools*²⁰, and photon phases were calculated using TEMPO2 (Hobbs et al. 2006) with the *fermi* plugin (Ray et al. 2011).

¹⁸ <https://wikio.nrao.edu/bin/view/CICADA/GUPPIUsersGuide>

¹⁹ <http://www.atnf.csiro.au/research/pulsar/tempo>

²⁰ <http://fermi.gsfc.nasa.gov/ssc/data/analysis/scitools/overview.html>

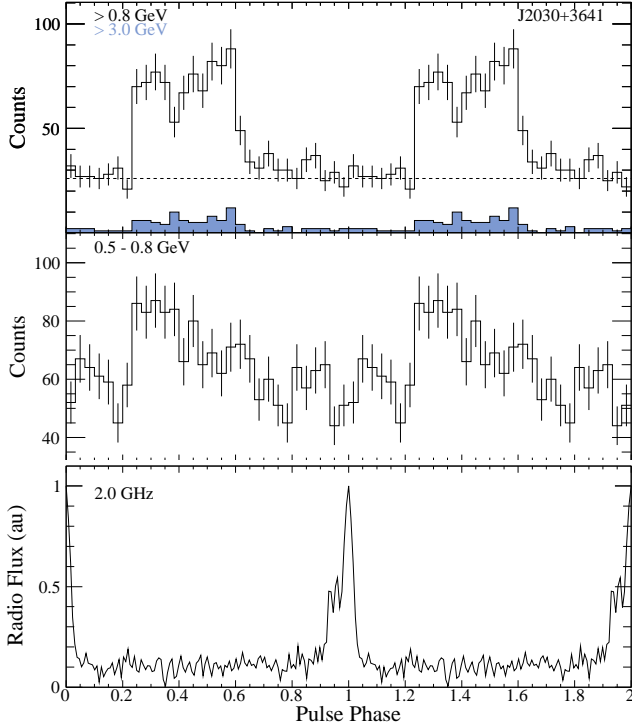


FIG. 2. — Phase-aligned radio and gamma-ray profiles of PSR J2030+3641. Bottom panel: discovery observation at the GBT. Middle panel: *Fermi* LAT 0.5–0.8 GeV profile (significant LAT pulsations are not detected below this energy band). Top panel: > 0.8 GeV and > 3 GeV (lower) LAT profiles. Each pulse profile is repeated in phase, and displayed with 30 bins per period in gamma rays and 128 bins in radio. The dashed line gives the level of unpulsed emission in the aperture as estimated from the light curve fits.

We first folded photons detected from 1FGL J2030.0+3641 based on the initial radio timing solution for PSR J2030+3641 (Section 2.2). Selecting photons using guesses for the minimum energy and radius of interest for extraction, we made a clear detection of pulsations. Optimal cuts in this region of very high background were subsequently found with $E > 0.8$ GeV and within a 0.5° radius. We then obtained 20 gamma-ray TOAs from a total of 1402 photons detected between 2008 August 4 and 2011 April 20 (49 days of integration per TOA), and used TEMPO2 to determine a timing solution with an rms of 4.0 ms. Despite the much higher precision of the individual radio TOAs, the best overall ephemeris is obtained by combining the gamma-ray and radio TOAs, owing to the longer span of the former. The parameters of this timing solution, in which a small amount of “timing noise” is parameterized by $\dot{\nu}$ (where $\nu = 1/P$), are presented in Table 1.

Figure 2 shows the gamma-ray pulse profiles in three energy bands, along with the radio discovery profile. In order to optimize each pulsed signal-to-noise ratio, we selected photons within 0.8° , 0.5° , and 0.3° of the timing position, respectively for the 0.5–0.8 GeV, > 0.8 GeV, and > 3 GeV bands. For the middle energy band, the bin-independent H-test (de Jager & Büsching 2010), with a value of 270, indicates enormous significance. For each of the other two bands, the H-test values of approximately 40 correspond to pulsation significances over 5σ . The light curve at > 0.8 GeV consists of two (conceivably three) overlapping components as observed, e.g., for PSRs J1709–4429, J1057–5226, and the CTA 1 pulsar (Abdo et al. 2010d), which have peak separation $\Delta \approx 0.25$. While the statistics are poor, the > 3 GeV profile is consistent

with such a description. At 0.5–0.8 GeV, only one peak is visible, which corresponds in phase with the first peak visible at higher energies. No pulsed signal was detected below 0.5 GeV, despite searches using different apertures. We fit the unbinned gamma-ray data above 0.8 GeV with two two-sided Gaussians, to account for the steep leading and trailing edges of the pulsed emission. The first peak is offset in phase from the main radio peak by $\delta = 0.26 \pm 0.02$ with $\text{FWHM} = 0.11 \pm 0.04$, while the second peak is offset from the first by $\Delta = 0.30^{+0.03}_{-0.08}$, with $\text{FWHM} = 0.18 \pm 0.05$. We have included systematic error from the modest uncertainty in DM and our choice of model.

2.3.1. Spectrum

To characterize the spectrum of PSR J2030+3641, we analyzed Pass 6 diffuse events collected between 2008 August 4 and 2011 April 20 selected to have reconstructed energies between 178 MeV and 100 GeV and reconstructed positions within 10° of the timing position of PSR J2030+3641. We excluded the 100–178 MeV energy bin because the rapidly increasing effective area in this bin exacerbates the effects of energy dispersion (Atwood et al. 2009). We removed events with a reconstructed zenith angle $> 100^\circ$ and also filtered data in which the aperture approached the limb of the Earth; these cuts remove most of the contribution of the bright gamma-ray emission produced by cosmic rays interacting in the Earth’s atmosphere. To further enhance the signal-to-noise ratio of PSR J2030+3641, we selected events with rotation phase $0.22 < \phi < 0.64$ (see Figure 2). We verified that there was negligible emission outside of this phase range, so the best-fit values may be taken to represent the phase-averaged magnetospheric emission.

PSR J2030+3641 lies in the source-crowded Cygnus region, and extracting its spectrum requires careful modeling of both neighboring point sources (including the three bright gamma-ray pulsars J2021+3651, J2021+4026, and J2032+4127) and the diffuse background. We included all point sources in a preliminary version of the 2FGL catalog (Abdo et al. 2011a) within 15° of the pulsar, as the broad point-spread function (PSF) at low energy allows sources away from the aperture boundary to contribute to the observed counts. Identified pulsars were modeled with a power law with exponential cutoff, $dN/dE \propto (E/\text{GeV})^{-\Gamma} \exp(-E/E_c)$. In the fits reported below, we varied all parameters for sources within 7° of the aperture, while sources outside of the aperture were held fixed at the catalog values. We modeled the Galactic and isotropic diffuse backgrounds using, respectively, the *gll_iem_v02_P6_V11_DIFFUSE* diffuse map and the *isotropic_iem_v02_P6_V11_DIFFUSE* tabulation employed for the 1FGL spectral analysis; these have been rescaled from those constructed with the *P6_V3_DIFFUSE* instrument response functions (IRFs). We allowed the normalizations of the diffuse models to vary in the fit.

We performed spectral fits with the *pointlike* application (Kerr 2011). This software bins the events in both energy and position, using HEALPix²¹ to provide position bins whose energy-dependent extent is always small compared to the PSF, providing a compact representation of the data with minimal information loss. We verified the results with the ScienceTool *gtlike*. The best-fit values are reported in Table 1, and include a power-law photon index $\Gamma = 1.1$ and cut-off energy

²¹ <http://healpix.jpl.nasa.gov/>

$E_c = 2.0$ GeV. These values apply to the profile as a whole, although Figure 2 suggests that the second gamma-ray peak has a harder spectrum than the first, as is observed for many gamma-ray pulsars (e.g., Abdo et al. 2011b).

In addition to the rescaled 1FGL diffuse model, we also performed the fit with an improved model internal to the LAT collaboration and with “Pass 7” data²² using the *P7SOURCE_V6* IRFs and the appropriate diffuse model (accompanying the 2FGL catalog). These values were consistent with those reported in Table 1, and the scatter has been used to estimate systematic errors on the parameters. We have also included uncertainty in the instrument’s effective area in the systematic errors through the use of “bracketing” IRFs (Abdo et al. 2009c).

2.4. X-ray Observations

A short *Swift* (Gehrels et al. 2004) observation was obtained on 2010 May 11 to search for an X-ray counterpart to PSR J2030+3641. No emission is observed at the pulsar position in this 3.8 ks X-ray Telescope (Burrows et al. 2005) PC mode observation, with a 3σ upper limit of 1.7×10^{-3} cts s^{-1} (0.5–8 keV). Assuming a power-law spectrum with photon index $\Gamma = 1.5$ for a possible pulsar wind nebula (e.g., Kargaltsev & Pavlov 2008) absorbed by a column with $N_H = 7.4 \times 10^{21}$ cm^{-2} (assuming one free electron for every 10 neutral hydrogen atoms along the line of sight), this corresponds to an unabsorbed flux limit of $f_X < 1.3 \times 10^{-13}$ erg cm^{-2} s^{-1} , or luminosity $L_X < 1.6 \times 10^{31} (d/1 \text{ kpc})^2$ erg s^{-1} . For a distance of ≈ 2 kpc (see Table 1), this corresponds to $L_X/\dot{E} < 2 \times 10^{-3}$, which is a reasonably stringent limit, although it would not be a surprise if the actual X-ray flux of this pulsar were about an order of magnitude below the current limit (see, e.g., Marelli et al. 2011).

3. DISCUSSION

The gamma-ray pulsations from PSR J2030+3641 unambiguously identify it as the origin of the gamma rays from 1FGL J2030.0+3641. We note also that a candidate TeV source possibly detected by the Milagro Gamma-Ray Observatory (“C2” in Abdo et al. 2007) is positionally coincident with PSR J2030+3641. Its faintness and location near a very bright source precludes further investigation based only on published results (see also Abdo et al. 2009d), but the relatively small \dot{E} and relatively large age and distance of PSR J2030+3641 make an association unlikely. With a DM-derived distance of 8 kpc, PSR J2030+3641 is located toward the Cygnus region, where until recently very few pulsars were known and where the pulsar distance scale is highly uncertain. Recent discoveries suggest that the Cordes & Lazio (2002) model greatly overpredicts distances in this direction: PSR J2032+4127, located 5° from PSR J2030+3641, with a DM-derived distance of 3.6 kpc, is thought to be located at half that distance (Camilo et al. 2009b); and PSR J2021+3651, less than 2° from PSR J2030+3641, with a model distance of 12 kpc, is more likely located at 2–4 kpc (Abdo et al. 2009e). Also, the RM for PSR J2030+3641 is large and positive, very similar to that of PSR J2021+3651, and this is suggestive of a location closer than the Perseus arm, at 6 kpc in this direction (see discussion in Han et al. 2006). Overall, we judge that a likely distance for PSR J2030+3641 is in the range 2–4 kpc.

²² See <http://fermi.gsfc.nasa.gov/ssc/data/analysis/scitools/>

3.1. Geometrical Constraints from Radio Profile

Johnston & Weisberg (2006) noted that the profiles of pulsars with high \dot{E} share many common features. In particular, the profiles with two components generally show (i) two components with equal width, (ii) the trailing component stronger than the leading component, (iii) close to 100% linear polarization, (iv) significant circular polarization under the trailing component, and (v) flat position angle swings which appear to steepen at the far trailing edge of the profile. The profile of PSR J2030+3641 conforms in some ways to these generalizations. The profile is symmetrical with the trailing edge brighter. The PA swing is remarkably flat with a hint of steepening at the trailing edge. However, although the leading component is highly polarized, the trailing edge is not, unlike the majority of the high \dot{E} pulsars. Weltevrede & Johnston (2008) pointed out that the transition between pulsars with low linear polarization and those which are highly polarized occurs at $\dot{E} \sim 10^{34.5}$ erg s^{-1} . PSR J2030+3641 could be an example of a pulsar in transition from high to low polarization.

The interpretation of these profiles by Johnston & Weisberg (2006) was that the magnetic pole crossing occurs at the (symmetry) center of the profile. The PA swing is significantly shifted to later phase because of aberration (Blaskiewicz et al. 1991), leading to emission heights close to 1000 km. This may also be the case in PSR J2030+3641. If we assume that the inflexion point of the PA swing is the rise in the PA curve some 20° after the profile center in Figure 1, this implies an emission height of ~ 800 km (close to 10% of the light cylinder), similar to those seen in other high \dot{E} pulsars. We also note that a height of ~ 800 km would in turn imply an overall pulse width of some 50° , similar to the observed value. This further suggests that the inclination between the magnetic and rotation axes cannot be too far from orthogonal.

3.2. Light Curve Fitting and Model Implications

We can use the gamma-ray light curve and polarimetric measurements to test the predictions of magnetosphere beaming models. Such tests are most constraining when the magnetic inclination angle α and the viewing angle ζ are well determined. The polarization data provide some geometrical constraints. Since the lower frequency data may be affected by interstellar scattering, our primary constraints are based on the 1.5 GHz data. We use PA values from the native 512 observational phase bins with $\sigma_{PA} < 10^\circ$ and phases $-0.1 < \phi < 0.05$ (relative to the intensity maximum; see Figure 1), and fit to a standard rotating vector model (RVM) polarization sweep. The maximum sweep rate is $d\Psi/d\phi|_{\max} = 1.4$ and one obtains good fits in a band of the α – ζ plane, with a best fit $\chi^2 = 37.5$ for 55 degrees of freedom (suggesting the PA errors are somewhat overestimated). Figure 3 shows the RVM fit confidence regions in this plane, after correcting for the RVM sign convention problem (Everett & Weisberg 2001). The phase of maximum sweep is not well constrained, but the best fits place it well after the radio peak at $\phi \approx 0.06$. The fit implies $\alpha < 140^\circ$, with best fit values $< 90^\circ$. If we simultaneously fit the 1.5 GHz points and the $-0.1 < \phi < 0.02$ 0.8 GHz data, larger $\alpha > 90^\circ$ are preferred, but this preference is controlled largely by the trailing edge of the sweep where scattering distortions may be present.

Following Romani & Watters (2010), we next compare the gamma-ray light curve to three geometrical models of outer magnetosphere emission. The first, “Outer Gap” (OG; Cheng et al. 1986), model posits emission from vacuum dipole field

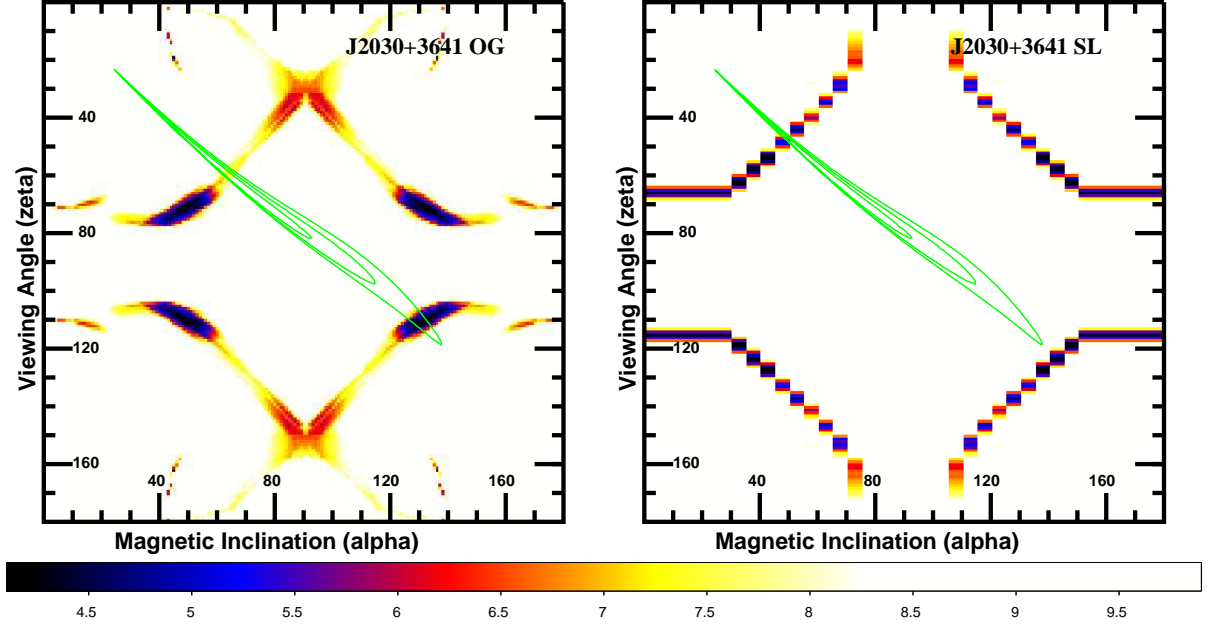


FIG. 3.— Surfaces of goodness of fit (χ_3) to the $E > 0.8$ GeV light curve for the OG (left) and SL (right) outer magnetosphere beaming models. Dark colors indicate lower (better) values of the fit statistic. The $\Delta\chi^2 = +1, +2, +3$ contours for the RVM fit to the 1.5 GHz polarization data are shown in green.

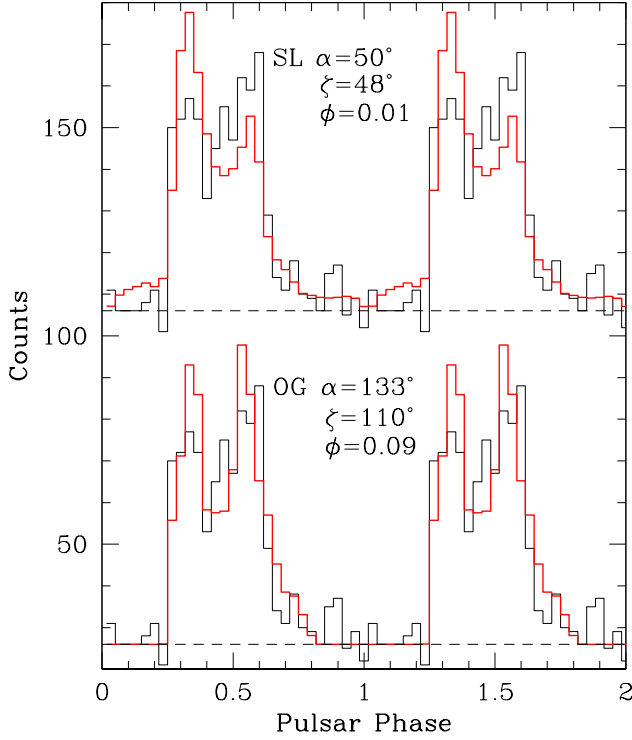


FIG. 4.— Model light curves (red) at the best-fit α and ζ consistent with the RVM PA constraints compared to the $E > 0.8$ GeV LAT light curve (black histograms). The offset ϕ indicates the phase of the closest approach of the magnetic dipole axis at the star surface. The SL curves have been offset by +80 counts/bin.

lines radiating from the null charge surface to the light cylinder at radius R_{LC} . In this model, the heuristic efficiency scaling $\eta \approx (10^{33} \text{ erg s}^{-1} / \dot{E})^{1/2}$ is assumed. For PSR J2030+3641, the value $\eta = 0.18$ was used for the gap width w in the OG calculations. The second model, “Two Pole Caustic” (TPC;

Dyks & Rudak 2003), has emission in the vacuum open zone from the neutron star surface out to $0.75 R_{LC}$ from the rotation axis or an altitude of R_{LC} , whichever is lesser. More recently, numerical models of force-free magnetospheres have been computed by Bai & Spitkovsky (2010) and they have argued that the pulsar gamma-ray beam can be created in the “Separatrix Layer” where the open zone current sheets overlap. The emission in this SL model is assumed to extend to $1.5 R_{LC}$. We assess the match to the data by plotting a goodness of fit χ_3 surface in the α - ζ plane (see Romani & Waters 2010). Using the $E > 0.8$ GeV light curve, the best-fit OG models (with best $\chi_3 = 3.9$ at $\alpha = 133^\circ$, $\zeta = 110^\circ$) lie inside the 3σ 1.5 GHz fit contours and at the maximum of the combined 1.5 GHz and 0.8 GHz fit. A small second region of adequate but poorer fits ($\chi_3 = 7$) is also present within the 1σ RVM contour at smaller $\alpha = 63^\circ$ ($\zeta = 60^\circ$). The SL model has a similar small region of good fits within the 1σ 1.5 GHz RVM contour ($\chi_3 = 5$ at $\alpha = 50^\circ$, $\zeta = 48^\circ$). The TPC model predicts a large unpulsed component resulting in much poorer fits (not shown), with a best value $\chi_3 = 19$ in the RVM-allowed region; this is at $\alpha = 26^\circ$, $\zeta = 25^\circ$, giving a light curve with little pulsed flux.

Figure 4 shows the best-fit light curves in the RVM-allowed region for the OG and SL models, compared with the data. The present models do not include the full radiation physics, employing simple uniform emissivity throughout the active zones. However, it appears that both high altitude models can produce reasonable matches to the LAT data. With improved geometrical constraints it may be possible to distinguish between the OG and SL models. For the former, the fit phase of the magnetic axis is at $\phi \approx 0.09$, after the pulse and somewhat later than the polarization sweep. The SL model prefers a magnetic axis much closer to the maximum of the radio pulse. In both cases, the lag of the sweep maximum from the pulse peak implies significant altitude ~ 0.1 – $0.15 R_{LC}$ for the radio emission. Such altitudes are also required to accommodate the relatively wide radio pulse in the open zone. Modeling

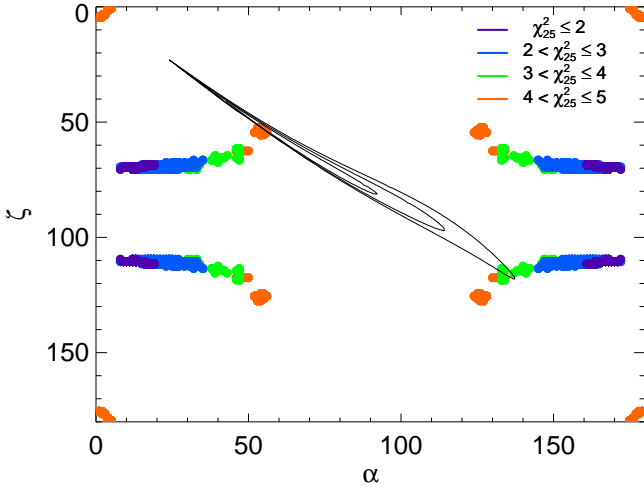


FIG. 5.— Reduced χ^2 values (with 25 degrees of freedom) in α – ζ space from slot gap gamma-ray light curve fits, marginalized over w , r , and $\Delta\phi$, and black curves from the RVM fit to radio polarization measurements, showing where these constraints intersect the geometrical light curve parameters (the overall best-fit light curve lies outside these regions; see Section 3.2). The plotted values of χ^2_{25} are those included in the Markov chains via the algorithm given in Verde et al. (2003).

such finite altitude effects may provide some additional restrictions on the geometry. We also note that the OG and SL models predict somewhat different viewing angles ζ ; if an X-ray pulsar wind torus could be measured, the resulting ζ might be used to select the preferred model.

The classic TPC model fails in these fits at least in part because it does not have enough emission at high altitudes. In order to improve upon this, we also fit the > 0.8 GeV profile of PSR J2030+3641 with light curves predicted from a geometrical high-altitude “Slot Gap” model (SG; Muslimov & Harding 2004), an evolution of the low-altitude SG of Muslimov & Harding (2003). In the SG geometry, the emission originates in a gap that extends from the neutron star surface at the polar cap to high altitudes near the light cylinder. We fit for four model parameters: α , ζ , gap width w (a fraction of the open volume radius of the polar cap, r_{ovc} , in the open volume coordinate system described in Dyks & Harding 2004), and maximum radius of emission r (in units of R_{LC}), assuming uniform emission rate in the corotating frame. Our resolution is 1° in α and ζ , $0.01 r_{\text{ovc}}$ in $0 \leq w \leq 0.3$, and $0.1 R_{\text{LC}}$ in $0.7 R_{\text{LC}} \leq r \leq 2.0 R_{\text{LC}}$ (we assumed a maximum cylindrical emission radius of $0.95 R_{\text{LC}}$). The simulated light curves are fit to the data via a Markov Chain Monte Carlo (MCMC) routine that explores the parameter space and records regions of maximum likelihood, as in Verde et al. (2003).

As noted before, we have some independent constraints on the emission geometry of PSR J2030+3641 from radio polarization (cf. Figure 1). To make our model fits be consistent with the RVM fit, we allowed the model light curve to shift with respect to the location of the magnetic pole by no more than $\Delta\phi = 0.1$ in phase. Figure 5 shows the α – ζ space with the polarization contours already shown in Figure 3 and color “contours” of reduced χ^2 from the MCMC likelihood fits. The polarization contours pass through parameters yielding light curve fits with $3 \leq \chi^2/25 \leq 5$, the best fit falling within the contours occurring at $(\alpha, \zeta, w, r, \Delta\phi; \chi^2/25) = (134^\circ, 114.5^\circ, 0.0 r_{\text{ovc}}, 1.4 R_{\text{LC}}, 0.08; 3.4)$. The second best fit that falls within the polarization contours is at $(54^\circ, 52.5^\circ, 0.01 r_{\text{ovc}}, 1.3 R_{\text{LC}}, 0.105; 4.2)$. We include this fit because while it has a larger χ^2 , it falls within a more constrained region of the

polarization contours. The absolute best fit, with or without restricting $\Delta\phi$, is at $(170^\circ, 110.5^\circ, 0.0 r_{\text{ovc}}, > 1.1 R_{\text{LC}}, 0.017; 1.4)$. This is inconsistent with standard radio cone beam emission because the values of α and ζ are too far apart for lower altitude radio emission to be visible. All of these light curves are shown in Figure 6.

Two of the fits include $w = 0$, meaning the emission in the model originates from a single open field line. Physically, this means the emission zone width is smaller than the resolution of our simulations, but not really zero. All the fits have small widths, requiring higher current of radiating particles in the gap (either more primaries or high pair multiplicity) in order to generate the observed luminosity. It is also likely that the emissivity and width of the emission zone change azimuthally and with altitude, unlike the constant width of our simulations (see Harding & Muslimov 2011). None of the fits are able to reproduce well the small middle peak of the observed light curve; it is not yet clear whether this is a separate feature or part of the second peak. Also, the background is slightly over-predicted by the SG model, especially for the parameters consistent with the polarization curves.

None of these (OG, SL, SG) gamma-ray light curve fits are particularly consistent with our inferences from the radio profile and polarimetric constraints. For instance, the latter suggest a nearly orthogonal rotator (Section 3.1), for which there are no good gamma-ray light curve fits. However, the polarimetric data provide limited constraints, owing to the small range of pulse longitude for which they are obtained, and our inferences rely on some assumptions. As for the gamma-ray fits, none are perfect, although the OG and SG fits appear slightly better than the SL one. Considering their inherent limitations, however, these fits are encouraging, and further refinements may improve our understanding of the magnetosphere of middle-aged pulsars like PSR J2030+3641.

For each beaming model, one can extrapolate the average pulsar flux on the Earth line-of-sight to the isotropic all-sky equivalent. For the best-fit angles consistent with polarization constraints, the corrections for PSR J2030+3641 are $f_\Omega = 0.66$ (OG), 0.64 (SL), and 0.78 (SG; neglecting polarization constraints, $f_{\Omega, \text{SG}} = 0.45$). Using the observed flux and the 8 kpc DM-estimated distance, we find that $\eta_{\text{obs}} = 4\pi d^2 f_\Omega F_\gamma / \dot{E} = 10 d_8^2 f_\Omega$. This indicates that any distance greater than ~ 2.5 kpc is problematic, unless the emission is highly beamed. For the OG/SL/SG beaming $f_\Omega \sim 0.7$, we require $d < 3$ kpc. The preferred distance for the heuristic OG efficiency law ($\eta = 0.18$) is ~ 1.3 kpc. Such distance estimates of ≈ 2 kpc are consistent with the discussion at the beginning of Section 3, and strongly suggest that PSR J2030+3641 is located at roughly $10\times$ the distance to Geminga ($d = 0.16$ kpc). Improved distance estimates for middle-aged, apparently efficient pulsars have the potential to constrain or falsify gamma-ray emission models.

3.3. Where Have All the (Ordinary Radio) Pulsars Gone?

In a radio search with the GBT of three unidentified low Galactic latitude LAT sources, we have discovered PSR J2030+3641, a relatively distant member of the under-represented group of gamma-ray pulsars that are middle-aged and have small \dot{E} . A gamma-ray-only pulsar was subsequently discovered in one of the two remaining sources, 1FGL J1746.7–3233 (Pletsch et al. 2011). The third source could yet be a gamma-ray pulsar, but is unlikely to be a substantial radio emitter beamed towards the Earth (assum-

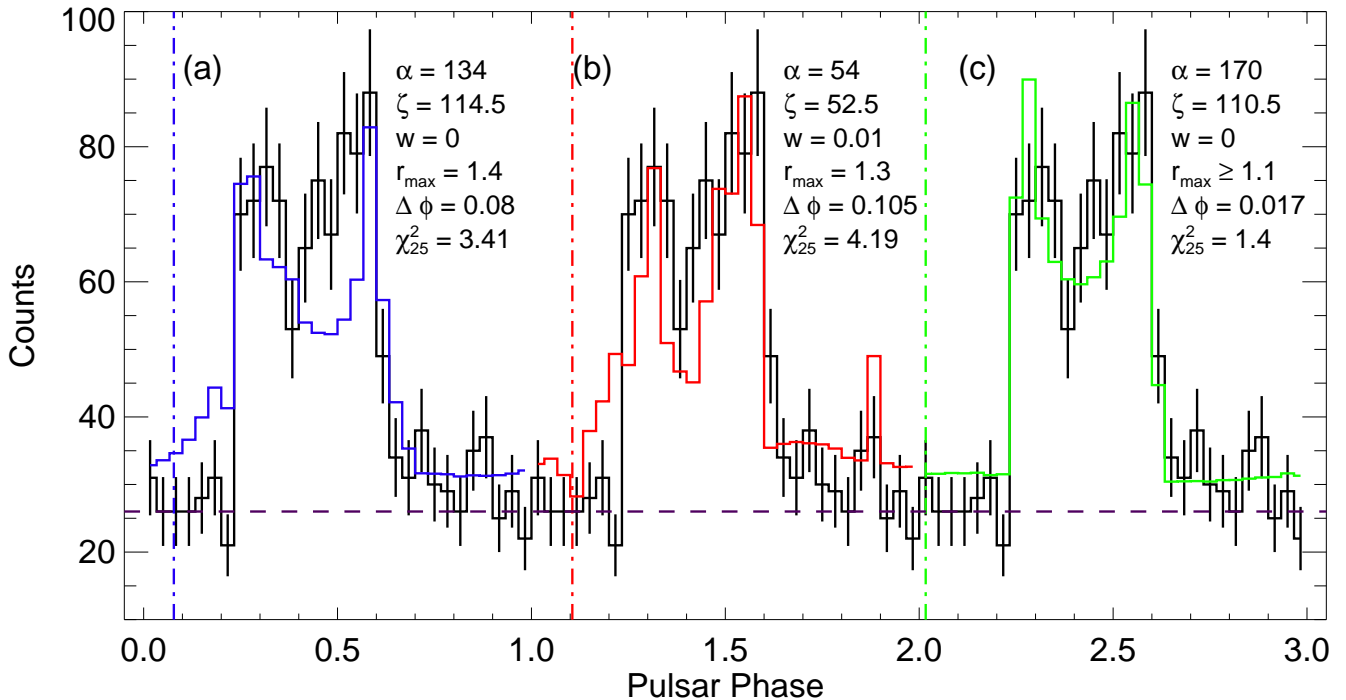


FIG. 6.— Slot gap model light curves compared to the data. (a) The best-fit light curve (blue) with parameters lying within the polarization contours. The LAT light curve is shown in black. The vertical dot-dashed line shows the model location of the magnetic pole, shifted by $\Delta\phi$ from zero. The horizontal dashed line represents the background count level. (b) Same as (a), for the second-best fit parameters (red). (c) Same as (a) and (b) for the absolute best-fit light curve (green) found by the MCMC routine, with no restriction on $\Delta\phi$. Its parameters do not fall within the radio polarization contours.

ing we covered its location adequately — in the case of 1FGL J1746.7–3233, the pulsar is $3/8$ offset from our GBT search position; see Section 2.1): for a fiducial distance of 4 kpc, our sensitivity corresponds to a luminosity limit $L_{1.4} \equiv S_{1.4}d^2 = 0.5$ mJy kpc², which is near the low end of the radio luminosity distribution for detected radio pulsars (see Abdo et al. 2010c; Camilo et al. 2009a,b, which include the two exceptions with much lower luminosities). It would seem that we were quite successful, with one related radio discovery among three LAT sources searched. However, as we argue next, we don’t expect such continued success.

Many more Galactic plane unidentified LAT sources have been searched for radio pulsars than the three mentioned here. This work is being done at the GBT, Parkes, Nançay, GMRT, and Effelsberg telescopes by members of the *Fermi* pulsar search consortium, and includes searches of all sources that have pulsar characteristics at all Galactic latitudes. So far this has resulted in the discovery of more than 30 MSPs, all at high latitudes (e.g., Cognard et al. 2011; Keith et al. 2011; Ransom et al. 2011) — and PSR J2030+3641. While a detailed population analysis will have to wait for the publication of all the completed searches, the lone example of PSR J2030+3641 already stands out. Why have more radio pulsars not been detected among the unidentified Galactic plane LAT sources?

A point related to this question concerns the very deep radio searches done of 34 pulsars discovered in blind pulsation searches of gamma rays (e.g., Abdo et al. 2009b; Pletsch et al. 2011; Saz Parkinson et al. 2010): only four of them were found to also be radio emitters (see Pletsch et al. 2011; Ray et al. 2011). Three are exceptionally faint and their detection was possible only following the gamma-ray discoveries (Abdo et al. 2010c; Camilo et al. 2009b; Pletsch et al. 2011). The remaining one, PSR J2032+4127 (Camilo et al. 2009b), is like PSR J2030+3641 in that they are both located

in the Cygnus region and both are relatively bright, being detectable in 1 minute with the GBT at 2 GHz. They were not known prior to the launch of *Fermi* simply because no sensitive surveys had (or have yet fully) been done of the northern (equatorial) reaches of the Galactic plane, using the high radio frequencies desired to unveil the Galactic disk. Conversely, the enormously successful 1.4 GHz Parkes multibeam survey (e.g., Manchester et al. 2001) *did* search the entire Galactic plane at $260^\circ < l < 50^\circ$ with sensitivity sufficient to detect ordinary (non-MSP) radio pulsars with $L_{1.4} \gtrsim 0.5$ mJy kpc² out to $d \gtrsim 2$ kpc. A very large fraction of all potentially detectable ordinary radio pulsars in that area of the sky that could also be plausible gamma-ray sources were therefore discovered before *Fermi* launch, especially when adding those discovered in deep pointed observations of known pulsar wind nebulae (e.g., Camilo et al. 2002). In time, several of these pulsars were detected by LAT (e.g., Abdo et al. 2010d). Subsequent to the Parkes multibeam survey an even deeper Parkes survey extended Galactic plane coverage out to $l = 60^\circ$ (Camilo et al., in preparation), and the on-going PALFA Arecibo survey is doing so out to $l \approx 75^\circ$ (Cordes et al. 2006).

In our view, the above suggests that the answer to “why have more radio pulsars not been detected among the unidentified Galactic plane LAT sources?” is that the vast majority of ordinary radio pulsars accessible to the current generation of telescopes and located within a few degrees of the plane at $l \lesssim 75^\circ$ that can yield an appreciable gamma-ray flux at the Earth were discovered a long time ago (it is possible that in rare but important cases very high L_γ distant pulsars will have their radio pulses scattered beyond practical detectability).

Many of the LAT sources that remain unidentified along the Galactic plane are surely pulsars — but they may not be detectable as radio sources, and should be searched anew in gamma rays (some of these may be in binaries, and inacces-

sible to current blind searches; see, e.g., Corbet et al. 2011). PSR J2030+3641 is bright enough that it would have been discovered in blind searches of 18 months of LAT data, if the photon selection criteria had been adjusted to take into account its flat spectrum (e.g., if only photons with $E \gtrsim 0.8$ GeV had been searched for pulsations), as we confirmed after discovery. Spectral analysis of a region can improve the signal-to-noise ratio by selecting events based on the probability that they come from the source of interest (see Belfiore 2011), and applying this technique to the Cygnus region also resulted in the unbiased detection of pulsations from PSR J2030+3641. For fainter point sources superimposed on the large and uncertain diffuse Galactic background, spectral analysis and localization are harder (1FGL J2030.0+3641 was only 0.4° from the actual pulsar position), but these and other improvements in search techniques are already resulting in the discovery of many more gamma-ray pulsars (see Pletsch et al. 2011; Saz Parkinson 2011). As a consequence, the ratio of known gamma-ray-only to gamma-ray-and-radio ordinary pulsars, which is currently slightly under 1.0, should increase substantially.

When will we ever learn all that we can (in the *Fermi* era) about the geometry and emission properties of gamma-ray and radio pulsar accelerators? Perhaps when full details emerge from the continuing collaborative radio and gamma-ray observational and modeling work. The future is bright (at some wavelength), but requires publication of all searches, including radio non-detections, and consideration of the non-detection by LAT of radio pulsars with very large \dot{E} flux at the

Earth (e.g., Romani et al. 2011).

The GBT is operated by the National Radio Astronomy Observatory, a facility of the National Science Foundation operated under cooperative agreement by Associated Universities, Inc. The *Fermi* LAT Collaboration acknowledges generous ongoing support from a number of agencies and institutes that have supported both the development and the operation of the LAT as well as scientific data analysis. These include the National Aeronautics and Space Administration (NASA) and the Department of Energy in the United States, the Commissariat à l’Energie Atomique and the Centre National de la Recherche Scientifique/Institut National de Physique Nucléaire et de Physique des Particules in France, the Agenzia Spaziale Italiana and the Istituto Nazionale di Fisica Nucleare in Italy, the Ministry of Education, Culture, Sports, Science and Technology (MEXT), High Energy Accelerator Research Organization (KEK) and Japan Aerospace Exploration Agency (JAXA) in Japan, and the K. A. Wallenberg Foundation, the Swedish Research Council and the Swedish National Space Board in Sweden. Support for this work was provided by NASA through Einstein Postdoctoral Fellowship Award Number PF0-110073 issued by the Chandra X-ray Observatory Center, which is operated by the Smithsonian Astrophysical Observatory for and on behalf of NASA under contract NAS8-03060.

Facilities: Fermi (LAT), GBT (GUPPI), Swift (XRT)

REFERENCES

- Abdo, A. A., et al. 2007, *ApJ*, 664, L91
— 2009a, *Science*, 325, 848
— 2009b, *Science*, 325, 840
— 2009c, *ApJ*, 696, 1084
— 2009d, *ApJ*, 700, L127
— 2009e, *ApJ*, 700, 1059
— 2010a, *ApJ*, 712, 957
— 2010b, *ApJS*, 188, 405
— 2010c, *ApJ*, 711, 64
— 2010d, *ApJS*, 187, 460
— 2011a, *ApJS*, submitted (arXiv/1108.1435)
— 2011b, *ApJ*, submitted (arXiv/1107.4151)
Arons, J. 1996, *A&AS*, 120, C49
Atwood, W. B., et al. 2009, *ApJ*, 697, 1071
Bai, X., & Spitkovsky, A. 2010, *ApJ*, 715, 1282
Belfiore, A. 2011, in *Radio Pulsars: an Astrophysical Key to Unlock the Secrets of the Universe*, ed. M. Burgay, N. D’Amico, P. Esposito, A. Pellizzoni, & A. Possenti, Vol. 1357 (AIP), 44
Blaskiewicz, M., Cordes, J. M., & Wasserman, I. 1991, *ApJ*, 370, 643
Burrows, D. N., et al. 2005, *Space Sci. Rev.*, 120, 165
Camilo, F., Manchester, R. N., Gaensler, B. M., & Lorimer, D. R. 2002, *ApJ*, 579, L25
Camilo, F., Ng, C.-Y., Gaensler, B. M., Ransom, S. M., Chatterjee, S., Reynolds, J., & Sarkissian, J. 2009a, *ApJ*, 703, L55
Camilo, F., et al. 2009b, *ApJ*, 705, 1
Cheng, K. S., Ho, C., & Ruderman, M. 1986, *ApJ*, 300, 500
Cognard, I., et al. 2011, *ApJ*, 732, 47
Corbet, R. H. D., et al. 2011, 1FGL J1018.6-5856: a new gamma-ray binary, ATEL 3221
Cordes, J. M., & Lazio, T. J. W. 2002, preprint (arXiv:astro-ph/0207156)
Cordes, J. M., et al. 2006, *ApJ*, 637, 446
de Jager, O. C., & Büsching, I. 2010, *A&A*, 517, L9
Dyks, J., & Harding, A. K. 2004, *ApJ*, 614, 869
Dyks, J., & Rudak, B. 2003, *ApJ*, 598, 1201
Everett, J. E., & Weisberg, J. M. 2001, *ApJ*, 553, 341
Gehrels, N., et al. 2004, *ApJ*, 611, 1005
Han, J. L., Manchester, R. N., Lyne, A. G., Qiao, G. J., & van Straten, W. 2006, *ApJ*, 642, 868
Harding, A. K., & Muslimov, A. G. 2011, *ApJ*, 726, L10
Hobbs, G. B., Edwards, R. T., & Manchester, R. N. 2006, *MNRAS*, 369, 655
Hotan, A. W., van Straten, W., & Manchester, R. N. 2004, *PASA*, 21, 302
Johnston, S., & Weisberg, J. M. 2006, *MNRAS*, 368, 1856
Kargaltsev, O., & Pavlov, G. G. 2008, in *American Institute of Physics Conference Series*, Vol. 983, 40 Years of Pulsars: Millisecond Pulsars, Magnetars and More, ed. C. Bassa, Z. Wang, A. Cumming, & V. M. Kaspi, 171–185
Keith, M. J., et al. 2011, *MNRAS*, 414, 1292
Kerr, M. 2011, PhD thesis, University of Washington, arXiv/1101.6072
Manchester, R. N., et al. 2001, *MNRAS*, 328, 17
Marelli, M., De Luca, A., & Caraveo, P. A. 2011, *ApJ*, 733, 82
Muslimov, A. G., & Harding, A. K. 2003, *ApJ*, 588, 430
— 2004, *ApJ*, 606, 1143
Pletsch, H. J., et al. 2011, *ApJ*, in press (arXiv/1111.0523)
Ransom, S. M. 2001, PhD thesis, Harvard University
Ransom, S. M., et al. 2011, *ApJ*, 727, L16
Ray, P. S., & Parkinson, P. M. S. 2011, in *High-Energy Emission from Pulsars and their Systems*, ed. D. F. Torres & N. Rea, 37 (arXiv/1007.2183)
Ray, P. S., et al. 2011, *ApJS*, 194, 17
Romani, R. W., Kerr, M., Craig, H. A., Johnston, S., Cognard, I., & Smith, D. A. 2011, *ApJ*, 738, 114
Romani, R. W., & Watters, K. P. 2010, *ApJ*, 714, 810
Saz Parkinson, P. M. 2011, in *Radio Pulsars: an Astrophysical Key to Unlock the Secrets of the Universe*, ed. M. Burgay, N. D’Amico, P. Esposito, A. Pellizzoni, & A. Possenti, Vol. 1357 (AIP), 48 (arXiv/1101.3096)
Saz Parkinson, P. M., et al. 2010, *ApJ*, 725, 571
Verde, L., et al. 2003, *ApJS*, 148, 195
Weltevred, P., & Johnston, S. 2008, *MNRAS*, 391, 1210

TABLE 1
MEASURED AND DERIVED PARAMETERS FOR PSR J2030+3641

Parameter	Value
Right ascension, R.A. (J2000.0)	20 ^h 30 ^m 00 ^s .261(4)
Declination, decl. (J2000.0)	36°41'27''15(7)
Galactic longitude, l (deg)	76.12
Galactic latitude, b (deg)	−1.44
Rotation frequency, ν (s^{-1})	4.99678736138(4)
Frequency derivative, $\dot{\nu}$ (s^{-2})	$-1.62294(5) \times 10^{-13}$
Frequency second derivative, $\ddot{\nu}$ (s^{-3})	$2.2(6) \times 10^{-24}$
Epoch of frequency (MJD)	55400.0
Dispersion measure, DM (pc cm ^{−3})	246.0(7)
Data span (MJD)	54700–55671
RMS timing residual (ms)	0.4
Spin-down luminosity, \dot{E} (erg s ^{−1})	3.2×10^{34}
Characteristic age, τ_c (yr)	4.9×10^5
Surface dipole magnetic field strength (Gauss)	1.2×10^{12}
Flux density at 2 GHz, S_2 (mJy)	0.09
Flux density at 1.5 GHz, $S_{1.5}$ (mJy)	0.15
Flux density at 0.8 GHz, $S_{0.8}$ (mJy)	0.40
Rotation measure, RM (rad m ^{−2})	$+514 \pm 1$
Radio–gamma-ray profile offset, δ (P)	0.26 ± 0.02
Gamma-ray profile peak-to-peak separation, Δ (P)	$0.30^{+0.03}_{-0.08}$
Gamma-ray (> 0.1 GeV) photon index, Γ	$1.1 \pm 0.2^{+0.2}_{-0.3}$
Gamma-ray cut-off energy, E_c (GeV)	$2.0 \pm 0.3^{+0.3}_{-0.4}$
Photon flux (> 0.1 GeV) (10^{-8} cm ^{−2} s ^{−1})	$3.6 \pm 0.5 \pm 0.8$
Energy flux (> 0.1 GeV), F_γ (10^{-11} erg cm ^{−2} s ^{−1})	$4.2 \pm 0.3 \pm 0.5$
DM-derived distance (kpc)	8
Most likely distance ^a , d (kpc)	1.5–3

NOTE. — Numbers in parentheses represent the nominal 1σ TEMPO2 timing uncertainties on the last digits quoted. For gamma-ray parameters, the first uncertainty is statistical and the second accounts for systematics (see Section 2.3.1).

^a See discussion at the beginning of Section 3 and at the end of Section 3.2.